Dynamics of the F 2 reaction with the simplest -bonding molecule

Yu-Ju Lu, Tingxian Xie, Jing-Wen Fang, Hua-Chieh Shao, and Jim J. Lin

Citation: The Journal of Chemical Physics **128**, 184302 (2008); doi: 10.1063/1.2913517
View online: http://dx.doi.org/10.1063/1.2913517
View Table of Contents: http://scitation.aip.org/content/aip/journal/jcp/128/18?ver=pdfcov
Published by the AIP Publishing

Dynamics of the F_2 reaction with the simplest π-bonding molecule

Yu-Ju Lu,[1] Tingxian Xie,[1,2] Jing-Wen Fang,[1,3] Hua-Chieh Shao,[1] and Jim J. Lin[1,4,a)]
[1]*Institute of Atomic and Molecular Sciences, Academia Sinica, Taipei 10617, Taiwan*
[2]*Department of Physics, Dalian Jiaotong University, Dalian, Liaoning 116028, People's Republic of China*
[3]*Department of Chemistry, National Taiwan University, Taipei 10617, Taiwan*
[4]*Department of Applied Chemistry, National Chiao Tung University, Hsinchu 30010, Taiwan*

(Received 25 February 2008; accepted 2 April 2008; published online 8 May 2008)

The reaction of $F_2+C_2H_4$ has been investigated with crossed molecular beam experiments and high level *ab initio* calculations. For a wide range of collision energies up to 11 kcal/mol, only one reaction channel could be observed in the gas phase. The primary products of this channel were identified as $F+CH_2CH_2F$. The experimental reaction threshold of collision energy was determined to be 5.5 ± 0.5 kcal/mol. The product angular distribution was found to be strongly backward, indicating that the reaction time scale is substantially shorter than rotation. The calculated transition state structure suggests an early barrier; such dynamics is consistent with the small product kinetic energy release measured in the experiment. All experimental results consistently support a rebound reaction mechanism, which is suggested by the calculation of the intrinsic reaction coordinate. This work provides a clear and unambiguous description of the reaction dynamics, which may help to answer the question why the same reaction produces totally different products in the condensed phase. © *2008 American Institute of Physics*. [DOI: 10.1063/1.2913517]

I. INTRODUCTION

Regarding the fluorination in organic chemistry,[1] $F_2+C_2H_4$ reaction is an important benchmark as it is the simplest reaction of F_2 with π-bonding systems. If this simple reaction can be understood, the mechanism may be extended to larger systems. Due to the small number of participating atoms, it should be feasible to study this reaction with high level *ab initio* calculations to reach a precision of the so-called chemical accuracy. Definitive experimental results of this reaction are also extremely desirable as to provide a test of the theories. Although there have been quite a number of experimental[2–11] and theoretical[12–19] investigations on the reaction of fluorine with ethylene, the reaction mechanism remains unclear. For convenience of discussion, we list three most likely primary product channels together with the calculated[20] reaction enthalpies:

$$F_2 + C_2H_4 \rightarrow C_2H_4F + F, \quad \Delta H^0_{0\ K} = -7.8 \text{ kcal/mol} \quad (R1),$$

$$\rightarrow C_2H_3F + HF, \quad \Delta H^0_{0\ K} = -100.4 \text{ kcal/mol} \quad (R2),$$

$$\rightarrow C_2H_4F_2, \quad \Delta H^0_{0\ K} = -118.5 \text{ kcal/mol} \quad (R3).$$

R1 has been observed in the gas phase.[2–4] The released F atom can initiate a series of exothermic chain reactions, which may lead to explosion. Kapralova *et al.*[2] reported the temperature dependence for R1 and showed the rate constant of reaction (1) can be expressed as follows:

$$k_1 = 8.0 \times 10^{-14} \exp(-E_a/RT) \text{ cm}^3 \text{ molecule}^{-1} \text{ s}^{-1},$$

and

$$E_a = 4.6 \text{ kcal/mol}.$$

Farrar and Lee[5] studied the decomposition of chemically activated C_2H_4F from $F+C_2H_4$ reaction in a crossed molecular beam setup. They employed a pyrolysis method to generate the F atom source from a F_2 gas mixture. The reactive signal of R1 was observed as a by-product from the reaction of C_2H_4 with the residue F_2 in their beam source.

For the $F_2+C_2H_4$ reaction in the condensed phase, investigations using the matrix isolation technique have provided some important results. Hauge *et al.*[6] studied the reactions of F_2 with a series of small hydrocarbons in F_2 or Ar matrices at 15 K. They concluded that propylene, butadiene, and cyclohexene reacted spontaneously with F_2 even at this low temperature; ethylene and allene reacted with F_2 when the matrix was exposed to infrared light in the wavelength range from 1 to 4 μm. For ethylene, the observed products were 1,2-difluoroethane (R3), vinyl fluoride and HF (R2). Neither the small alkane nor alkyne reacted, even exposed to the infrared light for a long time. Their results suggest that the activation energies of the F_2 reactions with these hydrocarbons may be in the order of propylene $\approx$ butadiene $\approx$ cyclohexene $<$ ethylene $\approx$ allene $<$ alkyne, alkane.

Frei and co-workers[7–10] investigated the infrared photoinduced reaction of $F_2 \cdot C_2H_4$ complex in N_2 or Ar matrices at 12 K. They excited various vibrational levels of C_2H_4 in the complex and monitored the reaction with Fourier-transform infrared absorption spectroscopy. Products of both R2 and R3 have been observed. The lowest excitation frequency which leads to the product formation is 1896 cm^{-1} (5.4 kcal/mol), indicating a reaction threshold. For vibra-

a)Electronic mail: jimlin@gate.sinica.edu.tw.

tional transitions between 1896 and 4209 cm^{-1}, deviations from a smooth rise of the quantum yield with energy have been attributed, in part, to mode selectivity. Similar HF/DF branching ratios close to 1.1 were found for the reactions of F_2 with three different isomers of $C_2H_2D_2$. Based on this observation, the contribution of an abstraction reaction of $F+C_2H_2D_2F$ to the HF(DF) formation was ruled out because at such a low temperature, the author expected significant isotope effect for the F atom attacking back on the CH or CD bond.[9] They concluded[7–10] that the $F_2+C_2H_4$ reaction under the cryogenic matrix-isolation conditions involves a vibrationally hot 1,2-difluoroethane intermediate, followed by a decomposition via either R2 or R3; the product branching ratio originates in a competition between the HF(DF) elimination and the thermal stabilization of the vibrational excited intermediate. The later process can be enhanced by two orders of magnitude with the addition of a second C_2H_4 in the matrix cage. It is less conclusive, however, for how the 1,2-difluoroethane intermediate is formed. Two possibilities have been mentioned: (i) a one-step four-center addition of F_2 to the C═C π-bond and (ii) a rapid sequential process within the same matrix cage, $F_2+C_2H_4 \rightarrow C_2H_4F+F \rightarrow C_2H_4F_2$.

Grover *et al.*[11] studied the reaction of F_2 with benzene in a crossed molecular beam experiment and determined the energy threshold of generating C_6H_6F+F products to be 13.9 ± 0.5 kcal/mol. The angular distribution of the C_6H_6F product was observed to be slightly backward with respect to the F_2 beam direction. The π electron system of benzene is more stable than that of C_2H_4 due to the resonance effect. Thus, a larger threshold for $F_2+C_6H_6$ reaction may be expected.

When reliable *ab initio* calculations were lacking, Raff[12] reported a semiempirical potential energy surface (PES) with the central structure being 1,2-difluoroethane, in which the barrier height of R3 was set to be 12.3 kcal/mol for the concerted, planar, four-center addition of F_2 across the ethylene double bond. A series of dynamic studies[13–15] have been performed on this PES for reactions in the gas phase and matrix-isolation conditions. Although this empirical PES yielded equilibrium geometries, reaction enthalpies, and fundamental vibrational frequencies in fair-to-good accord with experimental values, there was no reliable input for the properties of the transition states at that time.[12] Therefore, the results should be used with caution.

There have been some earlier ab initio investigations on $F_2+C_2H_4$ reaction but the employed calculation levels are probably not high enough to describe the reaction. Yamabe *et al.*[16] proposed a four-center transition state for a concerted $\alpha\beta$-addition using the Hartree–Fock and third-order Møller–Plesset calculations with 3-21G basis sets. The reported barrier is about 51 kcal/mol, which is even higher than the bond dissociation energy of F_2 (D_0=37 kcal/mol). Iwaoka *et al.*[17] suggested a nonconcerted mechanism with the MP2/6-31+G calculation, in which one C—F bond is formed first at the transition state structure. The calculated reaction barrier is 23 kcal/mol.

Recently, Wang *et al.*[18] investigated the mechanism for the addition of F_2 to C_2H_4 using density functional theory (DFT) with large basis sets. They proposed a two-step diradical mechanism: the first step is low-barrier attack of F_2 on C_2H_4 to produce a diradical intermediate of $F—F—CH_2—CH_2$ structure; the second step is the complete dissociation of the F—F bond, producing $F+CH_2F—CH_2$ (R1). For the first step, the obtained barrier height differs with the used functional; 1.8 kcal/mol using B3LYP and 6.3 kcal/mol with BHH (half-and-half functional). Qi *et al.*[19] studied this reaction with calculations of direct dynamics based on DFT and plane-wave basis sets. The authors found all three channels (R1, R2, and R3) in their simulations.

The abovementioned experimental and theoretical results in literature give rise to an immediate question as to why this reaction leads to totally different products in the gas phase than in the matrices which simulate a condensed phase surrounding. The chosen matrices consisted of N_2 or Ar, which should be inert enough in order to neglect chemical effects induced by the matrix itself. However, sterical caging effect in the condensed phase may be an important factor. Another arising question is: are the present theoretical calculations able to account for all the experimental observations? With this contribution, we would like to answer the above questions with crossed molecular beam experiments and high level *ab initio* calculations.

In our crossed molecular beam experiments, R1 was observed to be the only product channel for a wide range of collision energy up to 11 kcal/mol. The translational energy and angular distributions of the corresponding products were recorded. The collision energy threshold for the reaction was determined. In addition, possible reaction paths have been searched with high level *ab initio* calculations. Among the three possible primary channels, only a reaction path corresponding to R1 could be found under modest energy range. Energetics of R1 was determined using the CCSD(T) calculation extrapolated to the complete basis set limit (CBSL). The results obtained from various *ab initio* methods were compared and discussed. Combining the experimental and computational results, an unambiguous mechanism is given in this paper.

II. METHODS

A. Experimental

The experimental setup was similar to our previous works.[21,22] Therefore, only the essential parts of this experiment are given here. The F_2 molecular beam was generated by expanding 5% F_2/He mixture or neat F_2 gas (Spectra Gases, Inc.) through a fast pulsed valve[23] (Even-Lavie valve, high repetition rate model, ≤1000 Hz). The nozzle temperature was controlled to be at room temperature or a cryogenic temperature (~150 K) to generate different beam velocities. The mean speed of the neat F_2 beam was 700 m/s from the room temperature nozzle and 535 m/s from the cryogenic nozzle. The expansion of the seeded 5% F_2/He gas through the room temperature nozzle leads to a mean velocity of 1530 m/s.

The C_2H_4 gas (Linde, >99.99%) was seeded in He with two different concentrations of 4% and 10%. The gas mixtures were expanded through a similar pulsed valve to form

the molecular beams. To increase the beam speed, the respective nozzle is heatable. The C_2H_4 beam speed was tuned between 1500 and 1860 m/s by varying the seeding ratio and nozzle temperature. Both molecular beams were collimated by sharp-edge skimmers (Beam Dynamics, Inc.) to an angular divergence of about $\pm 1.3°$ [full width at half maximum (FWHM)].

Both molecular beams passed through further collimators cooled by a helium refrigerator and collided with each other under 90°. Following the reaction, the neutral products traveled a fixed distance to an ionizer. After ionization, the charged products were selected by a quadrupole mass filter and entered a Daly detector coupled with a multichannel scalar (MCS) (EG&G ORTEC) to do ion counting. The time-of-flight (TOF) spectra accumulated by the MCS were recorded and transferred into the product velocity distributions. The laboratory (LAB) frame angular distribution was obtained by integrating the TOF data for each given LAB angle. Scattering experiments of $Ar+C_2H_4$ and F_2+N_2 were performed to confirm that the observed signals in the $F_2+C_2H_4$ crossed beam experiments were not affected by the impurities in the F_2 and C_2H_4 samples.

To transform the data taken at the LAB frame to the center-of-mass (CM) frame, a forward convolution program was applied to simulate all TOF spectra and angular distribution. We input the experimental parameters (spreads of the beam velocities and flight distance, etc.) and iteratively adjusted the CM-frame translational energy distribution $P(E_T)$ and angular distribution $P(\theta_{CM})$ until a best fit was obtained. The Jacobian factor of the LAB-CM transformation has been included in the program.

The experimental studies were performed using two different apparatuses. The majority of the results presented here were obtained with the apparatus equipped with an electron-impact ionizer in the detector.[24] For measuring photoionization efficiency spectra, a second crossed molecular beam apparatus[25] coupled with the synchrotron radiation facility[26] was employed. The product flight distance is 10.1 cm in the synchrotron apparatus and 24.2 cm in the electron-impact apparatus. For a better velocity resolution, the TOF analysis was based on the electron-impact results.

For determination of the relative reaction cross section as a function of collision energy, the C_2H_4 and F_2 beam intensities need to be known. The C_2H_4 beam intensity was measured using a fast ionization gauge (Beam Dynamics, Inc.) operated at a reduced electron-impact energy (~23 eV) at which the He buffer gas produced no signal while C_2H_4 can still be efficiently ionized. The F_2 beam intensity could be deduced from the attenuation measurements, in which the C_2H_4 beam was slightly attenuated (<9%) by collisions of the F_2 beam.

B. *Ab initio* calculation

In this work, the complete active space self-consistent field (CASSCF) calculation with the second-order multireference perturbation theory (CASPT2) corrections[27–29] was used to explore the PES. It has been found that the CASPT2 calculation is computational efficient to predict not only the geometries of stable species but also transient structures along the reaction path.[30] We believe that it is important to use a multireference method to check the calculation of a reactive PES, especially when breaking/formation of a chemical bond is involved.

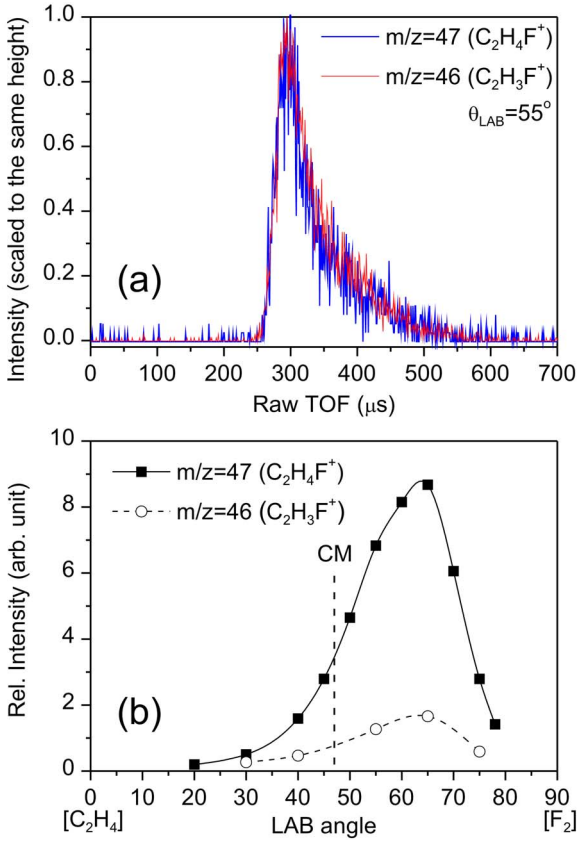

FIG. 1. (Color online) (a) A comparison of typical TOF spectra at m/z =47 and 46. The data were recorded with the electron-impact ionizer at 70 eV; (b) LAB-frame angular distributions of the reactive signals at m/z =47 and 46. The experimental data are connected with a spline fit for visualization. The corresponding : LAB angle of the center of mass is shown as a vertical dashed line. The data were recorded with the photoionization detector at 11 eV photon energy. The collision energy is 11.4 kcal/mol in both cases.

All calculations have been performed without setting the molecular symmetry, i.e., using the C_1 point group. This allows us to avoid unnecessary bias in choosing active orbitals. All employed active spaces have been carefully chosen and tested. The geometry optimization and zero point energy (ZPE) calculations were obtained mainly using the CASPT2 methods. Dunning basis sets[31,32] (cc-pV*N*Z and aug-cc-pV*N*Z, *N*=T, Q, 5) were employed. The barrier height and reaction enthalpy were obtained using single-point CCSD(T) calculations[33,34] based on the respective CASPT2 optimized geometries. The CCSD(T) energy was extrapolated to CBSL using the following scheme:[22] the Hartree–Fock energy was extrapolated with an exponential function, $\exp(-\gamma_1 N)$; the CCSD(T) correlation energy was extrapolated with a function[35] of $\gamma_2 N^{-3}$. Whenever the QCISD(T) analytical gradients[36] were available, the QCISD(T) approach was used to double-check the geometry optimization. All calculations were performed with the MOLPRO 2006.1 quantum chemistry package.[37]

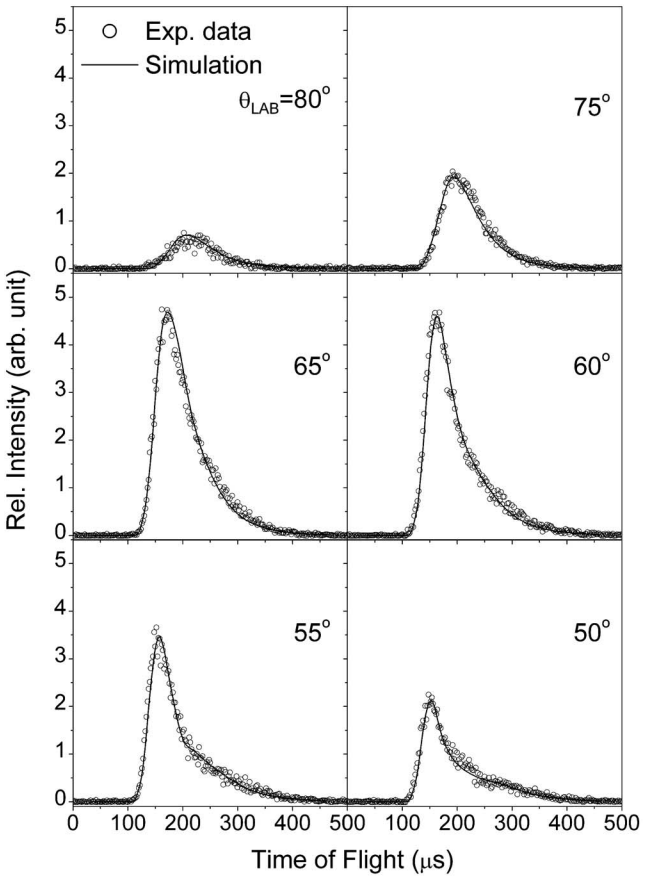

FIG. 2. TOF spectra of the C_2H_4F products from the $F_2+C_2H_4$ crossed beam reaction at 11.0 kcal/mol collision energy. The data were recorded at $m/z=46$ ($C_2H_3F^+$), which is a daughter ion of C_2H_4F. The molecular beam speeds used in the experiment were 1530 m/s for F_2 and 1840 m/s for C_2H_4; the corresponding LAB angle of the center of mass is about 48°. Here, the 0° in the LAB frame is defined as the C_2H_4 beam direction; the F_2 beam direction is at 90°.

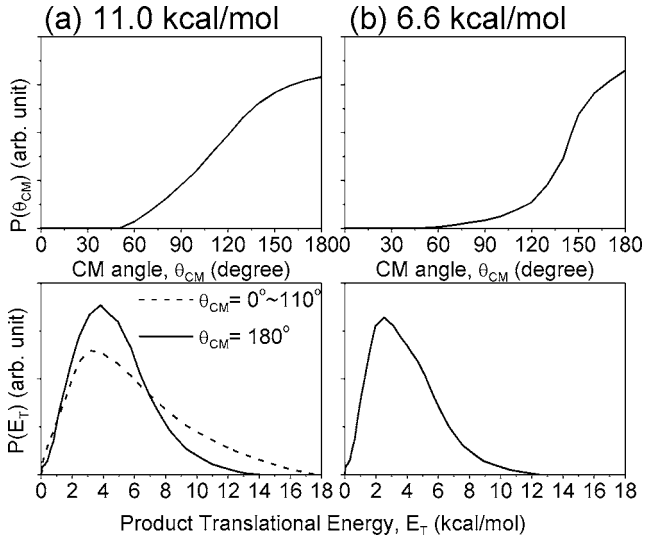

FIG. 3. CM-frame translational energy distribution $P(E_T)$ and angular distribution $P(\theta_{CM})$ used to simulate the R1 experimental data. (a) The collision energy is 11.0 kcal/mol. Slightly different $P(E_T)$ distributions were used for different CM angles; for CM angles in between 110° and 180°, an interpolated $P(E_T)$ was used. (b) The collision energy is 6.6 kcal/mol.

III. RESULTS

A. Crossed beam experiments

The first goal of this study is to identify the primary product channel(s) among the three possible ones: R1, R2, and R3. In the crossed molecular beam reaction of $F_2+C_2H_4$, we have searched for signals with the mass-to-charge ratios $m/z=47$, 46, and 66, which correspond to the parent masses of the possible products, C_2H_4F (R1), C_2H_3F (R2), and $C_2H_4F_2$ (R3), respectively. In the experiments, signals of reactive scattering could be observed at $m/z=47$ and 46. The existence of R1 can be verified with the observation of the $m/z=47$ signal. On the other hand, there are two likely contributions to the $m/z=46$ signal. One is from the C_2H_3F products of R2; the other is from dissociative ionization of the C_2H_4F (R1) product. For the latter case, the signal of the daughter ion usually has the same arrival time and angular distribution as its parent ion. A comparison of representative TOF spectra and LAB-frame angular distribution at $m/z=47$ and 46 is shown in Fig. 1. The identical shapes of TOF spectra and angular distributions strongly suggest that both masses are from the same neutral product C_2H_4F. The reaction energetics provide further evidence to discriminate R2. From the enthalpy of the reactions, it is obvious that the available energy of R2 products is much larger than that of R1 products. The translational energy release for producing two closed-shell molecules like $HF+C_2H_3F$ is usually large because the PES should be very repulsive in the exit valley. Therefore, the recoil velocity of the C_2H_3F product of R2 should be much larger than that of the C_2H_4F product of R1. The noise at earlier arrival times in the experimental TOF spectra is quite low, thus we can be sure that there is no faster product observed at $m/z=46$. Hence, the observed $m/z=46$ signal should stem from the dissociative ionization of the C_2H_4F product. Regarding the possibility of R3, its product angular distribution in the LAB frame will be very narrow because the recoil velocity is zero. Such hypothetical signal has not been observed in the crossed beam experiments. Again, energetically, the R3 product is unlikely to be observed in the gas phase because its exothermicity is larger than the energy required to break a chemical bond or to eliminate a HF molecule.

Figure 2 shows the experimental TOF spectra of the C_2H_4F product from the $F_2+C_2H_4$ crossed beam reaction at 11.0 kcal/mol collision energy. The ion of $m/z=46$, which is a daughter ion of the C_2H_4F product, was chosen because of its higher signal-to-noise ratio. Figures 1 and 2 show the product distributions in the LAB frame. In order to comprehend the underlying reaction dynamics, the experimental TOF data and angular distribution were transformed to the CM frame using the forward convolution method described in Sec. II A. The best-fit results in the CM frame are plotted in Fig. 3(a). Initially, one single $P(E_T)$ distribution was assumed to describe the entire dataset. However, the product scattered in the backward direction was consistently slower than at other CM angles. Therefore, a slower $P(E_T)$ for the backward direction ($\theta_{CM}=180°$) and a faster $P(E_T)$ for CM angles between 0° and 110° were used, connected by a linearly interpolated $P(E_T)$ distribution for the region between 110° and 180°. The resulting best fit for a collision energy of

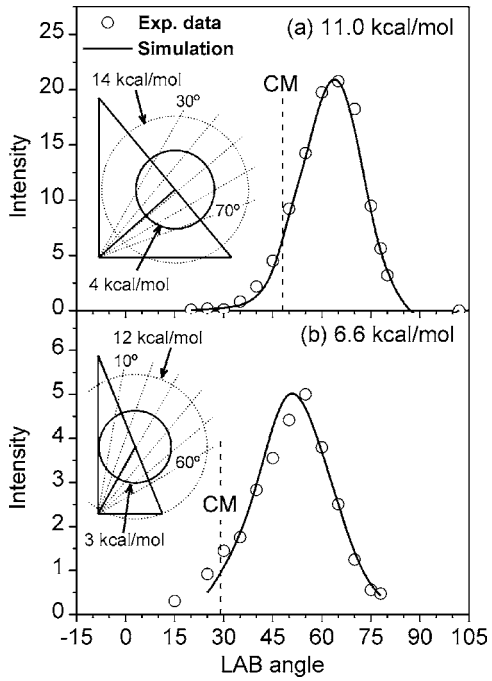

FIG. 4. The experimental and simulated LAB-frame angular distributions of R1 product signals with their schematic Newton diagrams. (a) E_c =11.0 kcal/mol; C_2H_4, 1840 m/s at 0°; F_2, 1530 m/s at 90°. (b) E_c =6.6 kcal/mol; C_2H_4, 1720 m/s at 0°; F_2, 700 m/s at 90°. In both panels, the corresponding LAB angle of the center of mass is shown as a vertical dashed line. The Newton circles represent the corresponding recoil velocities of the C_2H_4F product.

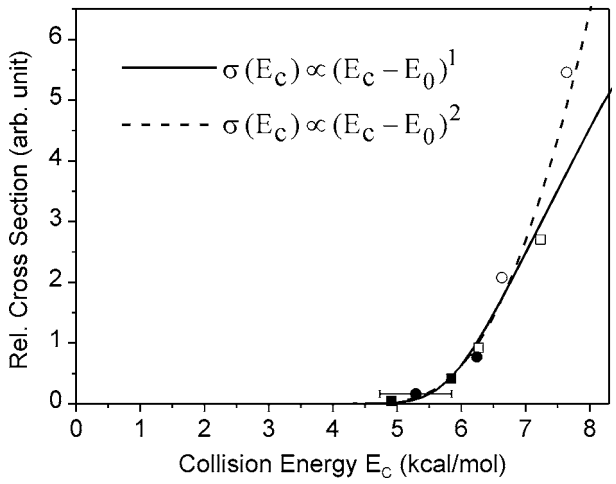

FIG. 5. The relative reaction cross section of R1 as a function of collision energy. Two functions convoluted with the collision energy spread are shown as the solid and dashed lines. The horizontal error bar indicates the width (FWHM) of the collision energy spread. Different symbols of the data points indicate the nozzle temperature used in the experiments: open/closed symbols for heated/RT C_2H_4 nozzle; square/circle symbols for cryo/RT F_2 nozzle (heated=413 K; RT=300 K; cryo=150 K).

6.6 kcal/mol is shown in Fig. 3(b). At this collision energy, we used only one $P(E_T)$ distribution to fit all of the TOF spectra recorded.

Figure 4 shows a comparison between the experimental and simulated LAB-frame angular distributions of the C_2H_4F product at 11.0 and 6.6 kcal/mol collision energies. Figure 4 clearly shows a highly asymmetric product angular distribution with a pronounced bias toward the LAB angles larger than that of the CM. Checking the LAB-frame angular distributions at several collision energies in the range of 5.3 to 11 kcal/mol always gave a similar trend. It is obvious from Figs. 3 and 4 that the CM-frame angular distributions are peaking preferentially in the backward direction.

No reactive signal could be found at collision energies smaller than 5.0 kcal/mol, while significant signals have been observed at higher collision energies. This threshold behavior is consistent with the previous gas-phase kinetic study[2] and matrix-isolation infrared-excitation investigations.[7–10] To determine the reaction threshold, the excitation function of R1, i.e., the relative reaction cross section as a function of collision energy was measured. The result is shown in Fig. 5, which was determined by the following procedure: (i) the LAB-frame angular distribution was measured at every selected collision energy; (ii) the peak height of the angular distribution was normalized with respect to both F_2 and C_2H_4 beam intensities. Then, the normalized peak height was plotted as a function of collision energy to give the data points in Fig. 5. This approach neglects the Jacobian factor of the LAB-CM transformation. However, we found that this factor varies very little within the collision energy range in Fig. 5. The resulting error of not including the Jacobian factor is less than 5%, thereby smaller than other experimental uncertainties. A more significant influence is the width of the collision energy. From the measured spreads of the molecular beam speeds, the width of the collision energy can be deduced. It is indicated as a horizontal error bar in Fig. 5. The experimental excitation function was fitted with two simple forms, a linear form $\sigma(E_c) \propto (E_c - E_0)^1$ or a quadratic form $\sigma(E_c) \propto (E_c - E_0)^2$, for the collision energy E_c higher than the threshold energy E_0. Both functions have been convoluted with the derived collision energy spread. The E_0 obtained are 5.8 ± 0.2 and 5.3 ± 0.3 kcal/mol for the linear and quadratic functions, respectively. Accounting for both results, we suggest the collision energy threshold for R1 to be 5.5 ± 0.5 kcal/mol.

To vary the molecular beam speed, we could heat the C_2H_4 nozzle to 413 K or cool the F_2 nozzle to 150 K. In order to check the influence of the nozzle temperature and the resulting change in vibrational distributions of the reactants, the experiment was designed to have conditions of different nozzle temperatures distributed in a narrow range of collision energy. In Fig. 5, the nozzle temperature combinations are indicated with different symbols as open/closed symbols for heated/RT C_2H_4 nozzle and square/circle symbols for cryo/RT F_2 nozzle (heated=413 K; RT=300 K; cryo=150 K). From these data, we cannot find any significant correlation with the nozzle temperature; all data points fall into a smooth line with deviations smaller than experimental uncertainties. This result indicates either the vibrational excitation in our molecular beams is negligible or its effect is too small to be observed.

B. Calculations

To further investigate the reaction mechanism of R1, the transition state was searched with the CASPT2 and QCISD(T) methods. For all CASPT2 results presented here,

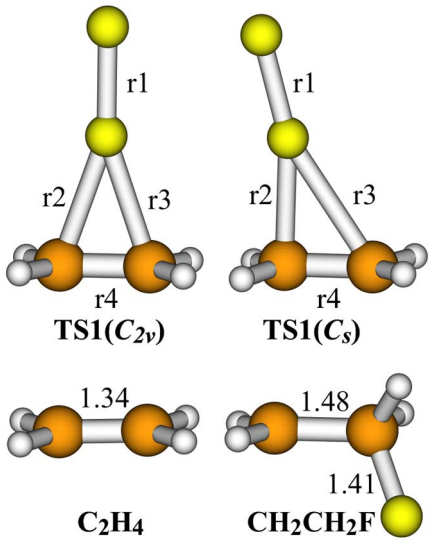

FIG. 6. (Color online) Optimized geometries of C_2H_4, CH_2CH_2F and the C_{2v} and C_s structures of the transition state (TS1). The C_2H_4 geometry was calculated with QCISD(T) using the basis sets: H=cc-pVDZ; C, F =aug-cc-pVTZ. The CH_2CH_2F geometry was calculated with CCSD(T) using the same basis sets. See Table I for details of TS1 structures. Unit: Å.

the active spaces have been carefully chosen to ensure that there is no orbital switching along the reaction paths and that the chemically important molecular orbitals such as the π/π^* orbitals of C_2H_4 and σ/σ^* orbitals of F_2 are included in the active spaces. Although we did not constrain the symmetry in the calculation (C_1 point group was used in all input files), two kinds of transition state (TS1) geometries were found for R1. The point groups of the two TS1 structures can be assigned as C_{2v} and C_s. The optimized geometries are shown in Fig. 6. Both C_{2v} and C_s structures of TS1 have been verified as a first-order saddle point on the PES. The vibrational frequency analysis for both structures shows that there is one imaginary frequency, of which the normal-mode displacement vector corresponds to the motions of the F—F bond dissociation and C—F bond formation.

Both C_{2v} and C_s geometries of TS1 can be located using CASPT2 calculations with different initial guess geometries. We have checked a few active spaces from [$(4e,4o)$ [four active electrons distributed in four active orbitals] to $(6e,8o)$. Selected results with important geometry parameters are listed in Table I. It can be seen in Table I that the active spaces have only little effect on the transition state geometry. For example, TS1a and TS1b are almost the same, and so are TS1c and TS1d. The QCISD(T) calculation predicts a C_s transition state (TS1 g) with a slightly longer r1 and slightly shorter r2, r3.

To check the effect of the augmented basis sets on the geometry calculation, a CASPT2(6e,6o) calculation was performed to locate the transition state with the basis sets: H =cc-pVDZ; C, F=aug-cc-pVTZ. The resulting geometry TS1e is very similar to TS1d with the largest difference in bond length to be only 0.04 Å. In addition, TS1f was obtained with larger basis sets on H. The resultant geometry is again very similar to TS1e. These results indicate that the type and size of the basis sets used have only minor effects on the TS1 geometry.

To clarify these C_{2v} and C_s structures of TS1, we performed single-point CCSD(T) calculations with the same basis sets. The results (see Table I) indicate practically no energy difference for these structures at the CCSD(T) level, independent of being of C_{2v} or C_s symmetry. We have also checked the single-point CCSD(T) energy for a few interpolated geometries between the C_{2v} and C_s structures. A smooth path connecting these two structures without any barrier could be obtained. These results indicate the PES is very flat in the region between the C_{2v} and C_s structures of TS1. It is important to mention that the product valley of R1 has to be a lower symmetry than C_{2v}. For the C_{2v} transition state, symmetry lowering is inevitable for product formation. We believe that the actual path of R1 may go though anyone of the C_{2v} and C_s transition state structures or any geometry between/near them. With the above argument of *symmetry lowering*, we have chosen the C_s structure of TS1 for the following discussions.

From TS1e, an intrinsic reaction coordinate (IRC) which connects TS1e to both reactant valley and product valley was obtained with a CASPT2 calculation [active space: $(6e,6o)$; basis sets: H=cc-pVDZ; C, F=aug-cc-pVTZ]. At each structure on the IRC, single-point energy calculations were per-

TABLE I. Comparison among TS1 geometries obtained with selected methods. Method of the geometry optimization: TS1a and TS1d: CAS-PT2(6e,6o)/cc-pVDZ (H), cc-pVTZ (C,F) with different initial guess geometries; TS1b: CAS-PT2(6e,8o)/cc-pVDZ (H), cc-pVTZ (C,F); TS1c: CAS-PT2(4e,4o)/cc-pVDZ (H), cc-pVTZ (C,F); TS1e: CAS-PT2(6e,6o)/cc-pVDZ (H), aug-cc-pVTZ (C,F); and TS1f: CAS-PT2(6e,6o)/cc-pVTZ (H), aug-cc-pVTZ (C,F); TS1g: QCISD(T)/cc-pVDZ (H), cc-pVTZ (C,F).

	Symmetry	E^b +277.74	r1	r2	r3	r4	∠FFC
TS1a	C_{2v}	−0.0034	1.650[a]	2.078		1.355	161.0
TS1b		−0.0033	1.654	2.075		1.357	160.8
TS1c	C_s	−0.0021	1.627	1.946	2.365	1.358	164.0
TS1d		−0.0021	1.628	1.947	2.356	1.358	163.8
TS1e		−0.0026	1.624	1.962	2.315	1.360	163.4
TS1f		−0.0029	1.620	1.985	2.325	1.357	163.2
TS1g		−0.0028	1.700	1.850	2.252	1.372	158.5

[a]Unit: Å and deg.
[b]Single-point energy calculated with CCSD(T)/cc-pVTZ (C,H); aug-cc-pVTZ (F). Unit: hartree. 1 hartree =627.5096 kcal/mol.

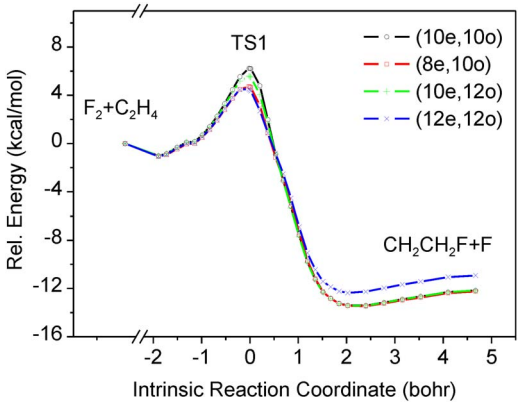

FIG. 7. (Color online) CASPT2 energy curves with various active spaces. The geometry points were obtained from the intrinsic reaction coordinate (IRC) calculation of TS1e with CASPT2(6*e*,6*o*)/cc-pVDZ (H); aug-cc-pVTZ (C,F).

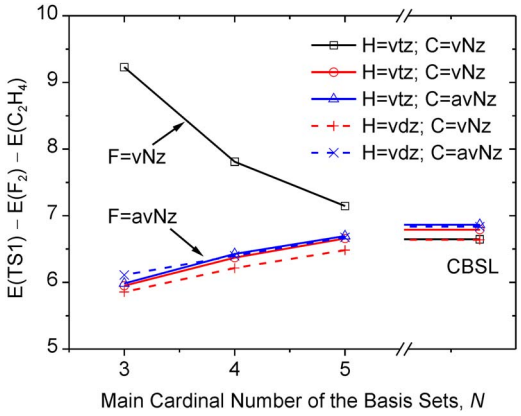

FIG. 8. (Color online) Basis set effects on the potential energy difference of TS1 to reactants. Single-point calculations were performed with CCSD(T) using various family of Dunning basis sets, noted as vNz=cc-pVNZ; avNz=aug-cc-pVNZ. TS1f geometry was used for TS1. CBSL=Complete basis set limit.

formed with larger active spaces up to $(12e,12o)$. The results are shown in Fig. 7. All relative energy curves in Fig. 7 have a similar shape but the barrier heights are slightly different. The lowest barrier height (ZPE not included) is about 4.6 kcal/mol for the CASPT2 calculations using $(8e,10o)$ and $(12e,12o)$ active spaces. The higher values are 5.6 and 6.2 kcal/mol for $(10e,12o)$ and $(10e,10o)$ active spaces, respectively.

With the results shown in Figs. 6 and 7, the reaction path of R1 can be described as a simple rebound type, in which one fluorine atom transfer is the major atomic motion along the reaction coordinate. A single barrier, separates the products from the reactants. It can be anticipated that the flux of the reaction is controlled by the TS1 barrier, acting as a kinetic bottleneck. To overcome this barrier, the favorable orientation of the approaching F_2 is roughly normal to the C_2H_4 molecular plane. The structure of the C_2H_4 subsystem varies little from the reactant valley to TS1, with a slightly elongated C—C bond distance for TS1. The analysis of the CASSCF molecular orbitals suggests the coupling of the $\pi\pi^*$ orbitals of C_2H_4 with the σ/σ^* orbitals of F_2 to be the most important interaction for the TS1 structure. On the IRC, there are van der Waals wells in both entrance and exit valleys. The well depths are about 1 kcal/mol, which is in the range of typical van der Waals interactions. The reaction is exothermic, i.e., the newly formed C—F bond is stronger than the F—F bond of F_2.

Figure 8 shows the effect of the basis sets on the TS1 barrier height (ZPE not included) at the CCSD(T) level. Five families of basis sets were tested. As can be seen in Fig. 8, the use of the augmented basis sets on fluorine has the most significant effect. For TS1, partial charge transfer to the F atoms was observed in the calculation. In this situation, the augmented basis sets are required to adequately describe the diffuse character of the atoms with (partially) negative charge. The quality of the basis sets is less crucial for the rest of atoms, especially for the H atoms as the CH bonding character varies only slightly along the IRC. In order to perform more efficient computation, relatively smaller basis sets were selected for the H atoms. If an extrapolation scheme is performed on the size of the basis sets for C and F atoms, the calculated potential energy barriers converge to about 6.8 kcal/mol (without ZPE correction) at all basis set selections.

The results of the ZPE calculations and CCSD(T) energies are summarized in Table II. The ZPE-corrected CBSL barrier height for TS1 is 7.8 kcal/mol or 7.1 kcal/mol using the individual CASPT2 or the QCISD(T) frequencies (not scaled), respectively. The lower value of 7.1 kcal/mol is still 1.6 kcal/mol higher than the experimental threshold of 5.5 ± 0.5 kcal/mol. This discrepancy seems significant and may locate on the borderline of the statistical CCSD(T) accuracy.[38,39] A possible source of error to account for this discrepancy lies in the ZPE calculation. The structure of the C_2H_4 subsystem of TS1 is quite similar to that of the reactant, suggesting the ZPE correction should be small. It is possible that the ZPE of TS1 is overestimated especially for the CASPT2 calculation, and/or that the harmonic approximation is not very good for TS1. As for the CCSD(T) energy, CCSD(T) is a single-reference based calculation, which may be less reliable if the electronic wave function of the studied system is of significant multireference character. For examining this issue, we have checked the value of the T_1 diagnostic of the CCSD(T) calculation. It has been recommended[40,41] that if T_1 is larger than 0.02, the results from single-reference electron correlation methods limited to single- and double-excitations should be viewed with caution, i.e., the CCSD calculation may be less reliable.[42] For the studied structures, T_1 is about 0.017 for TS1; 0.013 and 0.011 for F_2 and C_2H_4, respectively. The T_1 values are all small, suggesting that the single-reference methods such as CCSD, CCSD(T), and MP2 may be applicable. Nevertheless, although the discrepancy between the calculated and experimental reaction threshold seems significant, it is still in the reasonable range of statistical errors of CCSD(T) calculations. Other corrections, e.g., for core/valence and scalar relativistic effects and higher order correlation may improve the energy calculation at higher computational expense.[39] Moreover, for transitions states, the error estimation of an *ab initio* calculation is not well established yet.

Figure 9 shows the result of a two-state CASSCF calcu-

TABLE II. CCSD(T) results and zero-point energies for the reaction path of R1.

	Basis sets (N_H, N_C, N_F)[b]							
	(2,3,3)	(3,3,3)	(3,4,4)	(3,5,5)	CBSL[c]	CASPT2	QCISD(T)	Expt.
	Energy (hartree)						ZPE (hartree)[d]	
F_2	−199.3136	−199.3136	−199.3657	−199.3839	−199.3995	0.0021	0.0021	0.0021
C_2H_4	−78.4206	−78.4387	−78.4574	−78.4643	−78.4699	0.0506	0.0504	0.0492
CH_2CH_2F	−178.1208	−178.1390	−178.1839	−178.1999	−178.2135	0.0534		
F	−99.6278	−99.6278	−99.6529	−99.6616	−99.6690			
TSl[a]	−277.7248	−277.7429	−277.8129	−277.8375	−277.8585	0.0543	0.0530	
	Relative energy (kcal/mol)[e]						ΔZPE (kcal/mol)	
TS1 barrier	6.15	6.24	6.66	6.95	7.08	1.02	0.29	
$\Delta H^0_{0\ K}$	−8.42	−8.55	−8.12	−7.95	−7.81	0.48		

[a]Calculated at the TS1f geometry.
[b]Notation for the basis sets: H=cc-pVN_HZ; C=cc-pVN_CZ; F=aug-cc-pVN_FZ;
[c]CBSL=complete basis set limit. The Hartree–Fock energies were extrapolated with a function of $\exp(-\gamma_1 N)$. The CCSD(T) correlation energies were extrapolated with a function of $\gamma_2 N^{-3}$.
[d]ZPE=vibrational zero-point energy, which is calculated using the basis sets: H=cc-pVDZ; C=cc-pVTZ; F=aug-cc-pVTZ. The active spaces used for the CASPT2 calculations are $(6e,6o)$ for singlet species, and $(5e,5o)$ for doublet species. Experimental data are from Ref. 43.
[e]$\Delta ZPE_{QCISD(T)}$ is included in TS1 barrier; ΔZPE_{CASPT2} is used in $\Delta H^0_{0\ K}$.

lation along the same IRC in Fig. 7. Although the energy calculation at the CASSCF level is not very accurate, Fig. 9 provides qualitative potential energy curves of the ground state and the first excited state. The energy gap between these two electronic states is quite large at the reactant valley and becomes smaller for the product side. It is expected that there are degenerate electronic states at the product valley which consists of two radicals, $F+CH_2CH_2F$. The energy gap at the TS1 geometry is about 2.8 eV, suggesting a multireference calculation may not be necessary for TS1.

C. H-atom migration and photoionization efficiency spectrum

With the synchrotron facility, the photoionization efficiency (PIE) spectrum of the C_2H_4F product was measured at 9 kcal/mol collision energy. The corresponding ionization threshold was determined to be 8.9 eV from the abrupt rise of the PIE curve. Additionally, the PIE spectrum of C_2H_4 was also measured and the ionization threshold determined is in good accord with the literature value of 10.5 eV.[43] However, it is less straight forward to compare the experimental photoionization threshold of C_2H_4F to the result from a conventional *ab initio* calculation. We found that the ionic form of CH_2CH_2F is not a stable structure on the PES, which can isomerize to a more stable structure of CH_3CHF^+ without any barrier.[44,45] The experimental PIE signal usually corresponds to a photoionization process with a good Franck–Condon factor. A simple model of harmonic oscillators is not applicable in this case because the considered structure is very far from the equilibrium geometry. A fair description of the Franck–Condon factor and the interpretation of the PIE spectrum therefore require further theoretical investigation. On the neutral PES both isomers CH_2CH_2F and CH_3CHF are stable structures separated by a high barrier (see Fig. 10 for details). In our experimental conditions, the internal energy of the CH_2CH_2F product should be less than 20 kcal/mol, which is not enough for this H-atom migration process.

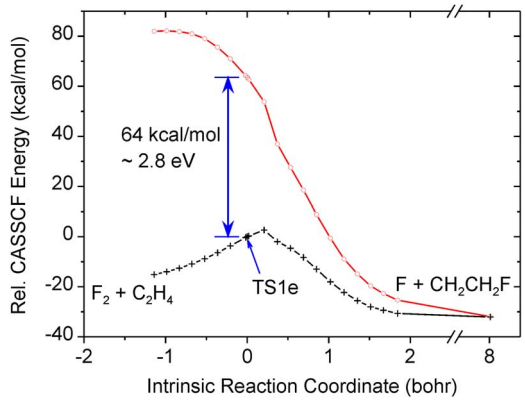

FIG. 9. (Color online) Two-state CASSCF potential energy curves calculated with $(10e,10o)$ active space. The geometries used are the same as those on the IRC shown in Fig. 7.

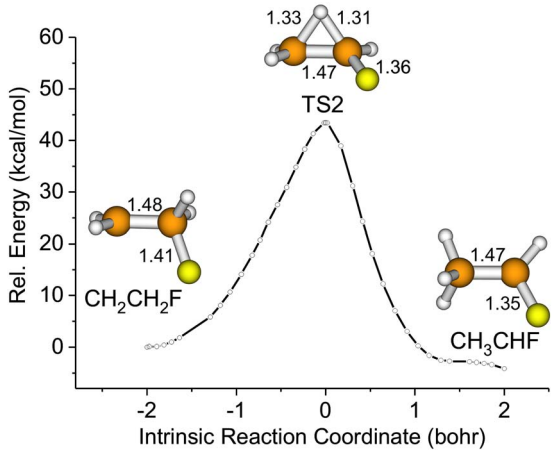

FIG. 10. (Color online) Potential energy curve on the intrinsic reaction coordinate (IRC) for the H-atom migration from the CH_2CH_2F product to CH_3CHF. Calculation method: CASPT2$(5e,5o)$/aug-cc-pVTZ.

IV. DISCUSSION

The average kinetic energy release (E_T) can be obtained from the product translational energy distribution $P(E_T)$. The total available energy E_{avl} for the R1 products is given by the sum of the collision energy and the reaction exothermicity of 7.8 kcal/mol. The fraction of the excess energy released as translation ($f_T=\langle E_T\rangle/E_{avl}$) was determined to be $f_T=0.27$ and $f_T=0.29$ for the collision energies of 6.6 and 11 kcal/mol, respectively. This means that more than 70% of the available energy is deposited into the product's internal degrees of freedom. In this reaction, the structure of TS1 was found to be more similar to the reactants than to the products. Thus, according to Polanyi's rule,[46,47] TS1 can be classified as an *early* barrier and the available energy is likely to excite the vibrational motion of the products. Polanyi's rule also suggests that a translational excitation of the reactants is more efficient in promoting the reaction than vibrational excitations. Although Polanyi's rule was initially proposed for a triatomic $A+BC$ reaction, it seems applicable to the $F_2+C_2H_4$ reaction because that the reaction path of R1 is very similar to a simple atom transfer reaction and the C_2H_4 subsystem is spectatorlike along the reaction path from the reactant valley to TS1. In addition, the equilibrium structure of the CH_2CH_2F product is quite different from the TS1 structure, also suggesting vibrational excitation of the products induced by the structure change in the exit valley.

The experimental angular distribution is highly asymmetric, indicating the reaction time scale is much shorter than the rotational period of the collision complex. This observation can clearly rule out the contribution of any long lifetime reaction intermediate such as 1,2-difluoroethane. The strongly backward distribution may be explained by a rebound mechanism.[47] For R1, head-on-like collisions with small impact parameters are more efficient to overcome the potential energy barrier; such collisions can lead to sharply backward products if the F—F—(C_2H_4) interaction lies on a linear line—an ideal rebound condition. The calculated TS1 geometry and energetics are in good agreement with this picture. Practically, there would be reasonable ranges for the impact parameters and cone of acceptance, resulting in the width of the product angular distribution. In brief summary, these results strongly indicate the following:

(i) the reaction time scale is much shorter than the complex rotation period;
(ii) collisions at small impact parameters dominate in the reactive events; and
(iii) the interaction between the three subunits, F, F, and (C_2H_4), is approximately linear.

Our reaction threshold of R1 is slightly higher than the reported activation energy of 4.6 kcal/mol obtained from a kinetic study in the temperature range of 300 to 430 K.[2] Under these comparably hot conditions, however, a thermal excitation of the F_2 vibration is possible to promote the reaction leading to the observed lower threshold. The fundamental vibrational frequency of F_2 is 894 cm^{-1}, corresponding to an energy gap of 2.55 kcal/mol. From the Boltzmann distribution, the ratio of $F_2(v=1)/F_2(v=0)$ can be estimated to be 5.0% at 430 K and 1.4% at 300 K. The increase in $F_2(v=1)$ population is quite significant when the temperature is raised above room temperature. It is very likely that the $F_2(v=1)+C_2H_4$ reaction has a significant lower threshold than the $F_2(v=0)+C_2H_4$ reaction. Therefore, the amount of thermal excitation of the reactants may have significant contribution to the empirical activation energy.

Wang *et al.*[18] studied the reaction with DFT calculations and proposed a diradical intermediate, which can be formed through a low barrier. The corresponding transition state has C_{2v} symmetry and its geometry (r1=1.794 Å; r2, r3 =1.975 Å; and r4=1.330 Å) is quite similar to our TS1a and TS1b. However, in the crossed beam experiments, we have observed highly asymmetric product angular distribution, indicating the reaction time scale is substantially shorter than rotation. This finding does not support the mechanism of a stable intermediate. The stability of the *diradical* may be too small to have a significant effect. In Fig. 7, a van der Waals well can be seen in the product valley but the well depth is quite shallow in comparison with the DFT results[18] of 5.6 kcal/mol (B3LYP) or 4.0 kcal/mol (BHH). We believe that the multireference CASPT2 calculation should provide a better description than the DFT calculations for the exit valley which has significant diradical character. On the other hand, from the product valley, it is quite feasible to form the structure of 1,2-difluoroethane if the ejected F atom is let to attack back to the radical site (the unpaired electron on the carbon atom) of the CH_2CH_2F. In the gas phase, there is essentially very little probability for this process but it should be quite likely in the condensed phase. Cage effect in high density environments, such as a cryogenic matrix, effectively hinders the escape of the F atom. The $F+CH_2CH_2F$ reaction is a typical process of radical-radical recombination which is usually barrierless. Therefore, R3 product may be formed through this sequential process following R1. The initially produced 1,2-difluoroethane is highly vibrationally excited. It can decompose to $HF+CH_2CHF$ or be stabilized through efficient energy transfer in the condensed phase. In this study, a detailed computational search for a direct reaction path related to either concerted addition (R3) or HF formation (R2) led to no results. Combining these theoretical efforts with the experimental observation that only R1 is observed in the gas phase, we strongly suggest that R2 and R3 observed in the condensed phase are most likely due to the cage effect and fast sequential reactions following R1.

V. SUMMARY

The $F_2+C_2H_4$ reaction has been investigated with crossed molecular beam experiments and high level *ab initio* calculations in detail. R1 has been found to be the only primary product channel in the gas phase. The experimental reaction threshold has been determined to be 5.5 ± 0.5 kcal/mol. The translational energy and angular distributions of R1 products have been recorded. The strongly backward angular distribution indicates a typical rebound reaction mechanism discriminating mechanisms involving a stable intermediate. The calculated transition state of R1 can be classified as an earlier barrier, which is consistent with the

small fraction of product translational energy release ($f_T \cong 0.28$) observed in the experiments. The reaction path of R1 has been calculated while other concerted-addition paths could not be found. The previous condensed-phase results can be explained by secondary reactions following R1 due to the cage effect.

Our ongoing research includes F_2 reactions with other unsaturated hydrocarbons such as C_3H_6, C_4H_8, and C_2H_2. Preliminary results show that the barriers for the F_2 reactions with C_3H_6 and C_4H_8 are significantly lower than that of $F_2+C_2H_4$ reaction, while the $F_2+C_2H_2$ reaction has a much higher barrier. A direct formation of HF could not been observed in either of these reactions.

ACKNOWLEDGMENTS

National Science Council (Grant No. NSC95-2113-M-001-041-MY3) and Academia Sinica, Taiwan supported this work. We thank Professor Yuan T. Lee and Dr. Jens Riedel for valuable comments and National Synchrotron Radiation Research Center, Taiwan for the use of facilities.

[1] For example, see R. D. Chambers, *Fluorine in Organic Chemistry* (Blackwell, Oxford, 2004); M. Sawaguchi, S. Hara, and N. Yoneda, J. Fluorine Chem. **105**, 313 (2000); S. Rozen, Acc. Chem. Res. **21**, 307 (1988); S. T. Purrington, B. S. Kagen, and T. B. Patrick, Chem. Rev. (Washington, D.C.) **86**, 997 (1986); R. F. Merritt, J. Am. Chem. Soc. **89**, 609 (1967).
[2] G. A. Kapralova, A. M. Chaikin, and A. E. Shilov, Kinet. Katal. **8**, 421 (1967).
[3] Z. K. Gyul'bekyan, O. M. Sarkisov, and V. I. Vedeneev, Kinet. Katal. **15**, 993 (1974).
[4] V. L. Orkin and A. M. Chaikin, Kinet. Katal. **23**, 438 (1982).
[5] J. M. Farrar and Y. T. Lee, J. Chem. Phys. **65**, 1414 (1976).
[6] R. H. Hauge, S. Gransden, J. L.-F. Wang, and J. L. Margrave, J. Am. Chem. Soc. **101**, 6950 (1979).
[7] H. Frei, L. Fredin, and G. C. Pimentel, J. Chem. Phys. **74**, 397 (1981).
[8] H. Frei and G. C. Pimentel, J. Chem. Phys. **78**, 3698 (1983).
[9] H. Frei, J. Chem. Phys. **79**, 748 (1983).
[10] H. Frei and G. C. Pimentel, Annu. Rev. Phys. Chem. **36**, 491 (1985).
[11] J. R. Grover, Y. Wen, Y. T. Lee, and K. Shobatake, J. Chem. Phys. **89**, 938 (1988).
[12] L. M. Raff, J. Phys. Chem. **91**, 3266 (1987).
[13] L. M. Raff, J. Phys. Chem. **92**, 141 (1988).
[14] L. M. Raff, J. Chem. Phys. **93**, 3160 (1990).
[15] L. M. Raff, J. Chem. Phys. **95**, 8901 (1991).
[16] S. Yamabe, T. Minato, and S. Inagaki, J. Chem. Soc., Chem. Commun., 532 (1988).
[17] T. Iwaoka, C. Kaneko, A. Shigihara, and H. Ichikawa, J. Phys. Org. Chem. **6**, 195 (1993).
[18] B.-W. Wang, L. Chan, S. P. Chan, Z.-D. Chen, and Z.-F. Liu, J. Chem. Phys. **120**, 9467 (2004).
[19] Y. Qi, K.-L. Han, and A. J. C. Varandas, Chin. J. Chem. Phys. **20**, 109 (2006).
[20] The electronic energy U is calculated with the CCSD(T) method at the complete basis set limit for R1 (see Table II) and at the basis sets: H=cc-pVTZ; C=cc-pVQZ; F=aug-cc-pVQZ for R2 and R3. The vibrational zero-point energy is calculated with the CASPT2 methods. $\Delta H^0_{0\ \mathrm{K}}=\Delta U+\Delta \mathrm{ZPE}$. See Table II for details.
[21] Y.-J. Lu, L. Lee, J.-W. Pan, H. A. Witek, and J. J. Lin, J. Chem. Phys. **127**, 101101 (2007).
[22] Y.-J. Lu, L. Lee, J.-W. Pan, T. Xie, H. A. Witek, and J. J. Lin, J. Chem. Phys. **128**, 104317 (2008).
[23] U. Even, J. Jortner, D. Noy, and N. Lavie, J. Chem. Phys. **112**, 8068 (2000).
[24] J. J. Lin, D. W. Hwang, S. Harich, Y. T. Lee, and X. Yang, Rev. Sci. Instrum. **69**, 1642 (1998).
[25] J. J. Lin, Y. Chen, Y. Y. Lee, Y. T. Lee, and X. Yang, Chem. Phys. Lett. **361**, 374 (2002).
[26] See: http://140.110.203.42/bldoc/21AU9WL.htm or www.nsrrc.org.tw.
[27] H.-J. Werner, Mol. Phys. **89**, 645 (1996).
[28] P. Celani and H.-J. Werner, J. Chem. Phys. **112**, 5546 (2000).
[29] P. Celani and H.-J. Werner, J. Chem. Phys. **119**, 5044 (2003).
[30] L. B. Harding, S. J. Klippenstein, and A. W. Jasper, Phys. Chem. Chem. Phys. **9**, 4055 (2007).
[31] T. H. Dunning, Jr., J. Chem. Phys. **90**, 1007 (1989).
[32] R. A. Kendall, T. H. Dunning, Jr., and R. J. Harrison, J. Chem. Phys. **96**, 6796 (1992).
[33] M. J. O. Deegan and P. J. Knowles, Chem. Phys. Lett. **227**, 321 (1994).
[34] P. J. Knowles, C. Hampel, and H.-J. Werner, J. Chem. Phys. **99**, 5219 (1993); J. Chem. Phys. **112**, 3106(E) (2000).
[35] T. Helgaker, W. Klopper, H. Koch, and J. Noga, J. Chem. Phys. **106**, 9639 (1997).
[36] G. Rauhut and H.-J. Werner, Phys. Chem. Chem. Phys. **3**, 4853 (2001).
[37] H.-J. Werner, P. J. Knowles, R. Lindh *et al.*, MOLPRO, Version 2006.1, a package of *ab initio* programs (see http://www.molpro.net).
[38] T. Helgaker, T. A. Ruden, P. Jørgensen, J. Olsen, and W. Klopper, J. Phys. Org. Chem. **17**, 913 (2004).
[39] D. Feller and K. A. Peterson, J. Chem. Phys. **126**, 114105 (2007).
[40] T. J. Lee and G. E. Scuseria, in *Quantum Mechanical Electronic Structure Calculations with Chemical Accuracy*, edited by S. R. Langhoff (Kluwer, Dordrecht, 1995), pp. 47–108.
[41] T. J. Lee and P. R. Taylor, Int. J. Quantum Chem., Symp. **23**, 199 (1989).
[42] For CCSD(T), T_1 slightly larger than 0.02 may be acceptable, but there is no recommended critical value of T_1 for CCSD(T) calculations in the literature.
[43] See: http://webbook.nist.gov/cgi/cbook.cgi?ID=C74851&Units=SI&Mask=20#Ion-Energetics.
[44] Calculated with B3LYP, MP2, QCISD, and CASPT2 methods using cc-pVTZ basis sets.
[45] Experimental adiabatic ionization energy of CH_3CHF is 7.93 eV; See: http://webbook.nist.gov/cgi/cbook.cgi?ID=C52067193&;Units=SI&Mask=20#Ion-Energetics.
[46] J. C. Polanyi, Acc. Chem. Res. **5**, 161 (1972).
[47] R. D. Levine, R. B. Bernstein, *Reaction Dynamics and Chemical Reactivity* (Oxford University Press, Oxford, 1987).